Published in final edited form as:
Dalton Trans. 2011 February 7; 40(5): 1119–1131. doi:10.1039/c0dt00871k.

Chalcogenidobis(ene–1,2–dithiolate)molybdenum(IV) complexes (chalcogenide E = S, Se): Probing Mo≡E and ene–1,2–dithiolate substituent effects on geometric and electronic structure†

Hideki Sugimoto[a], **Hiroyuki Tano**[b], **Koichiro Suyama**[b], **Tomoya Kobayashi**[b], **Hiroyuki Miyake**[b], **Shinobu Itoh**[a], **Regina P. Mtei**[c], and **Martin L. Kirk**[c]

Hideki Sugimoto: sugimoto@mls.eng.osaka-u.ac.jp; Shinobu Itoh: shinobu@mls.eng.osaka-u.ac.jp; Martin L. Kirk: mkirk@unm.edu

[a]Department of Material and Life Science, Graduate School of Engineering, Osaka University, 2-1 Yamada-oka, Suita, Osaka 565-0871*Japan*

[b]Department of Chemistry, Graduate School of Science, Osaka City University, 3-3-138 Sumiyoshi-ku, Osaka 558-8585, *Japan*

[c]Department of Chemistry and Chemical Biology, The University of New Mexico, MSC03 2060, 1 University of New Mexico, Albuquerque, New Mexico 87131–0001, *USA*

Abstract

New square–pyramidal bis(ene–1,2–dithiolate)MoSe complexes, $[Mo^{IV}Se(L)_2]^{2-}$, have been synthesised along with their terminal sulfido analogues, $[Mo^{IV}S(L)_2]^{2-}$, using alkyl (L^{C4H8}), phenyl (L^{Ph}) and methyl carboxylate (L^{COOMe}) substituted dithiolene ligands (L^{R}). These complexes now complete three sets of $Mo^{IV}O$, $Mo^{IV}S$ and $Mo^{IV}Se$ species that are coordinated with identical ene–1,2–dithiolate ligands. The alkyl substituted $[Mo(S/Se)(L^{C4H8})_2]^{2-}$ complexes were reported in prior investigations (H. Sugimoto, T. Sakurai, H. Miyake, K. Tanaka and H. Tsukube, *Inorg. Chem*. 2005, **44**, 6927, H. Tano, R. Tajima, H. Miyake, S. Itoh and H. Sugimoto, *Inorg. Chem*. 2008, **47**, 7465). The new series of complexes enable a systematic investigation of terminal chalcogenido and supporting ene–1,2–dithiolate ligand effects on geometric structure, electronic structure, and spectroscopic properties. X–ray crystallographic analysis of these $(Et_4N)_2[Mo(E)L_2]$ (E = terminal chalcogenide) complexes reveals an isostructural Mo centre that adopts a distorted square pyramidal geometry. The M≡E bond distances observed in the crystal structures and the ν(M≡E) vibrational frequencies indicate that these bonds are weakened with an increase in L→Mo electron donation ($L^{COOMe} < L^{Ph} < L^{C4H8}$), and this order is confirmed by an electrochemical study of the complexes. The ^{77}Se NMR resonances in MoSeL complexes appear at lower magnetic fields as the selenido ion became less basic from $MoSeL^{C4H8}$, $MoSeL^{Ph}$ and $MoSeL^{COOMe}$. Electronic absorption and resonance Raman spectroscopies have been used to assign key ligand-field, MLCT, LMCT and intraligand CT bands in complexes that possess the L^{COOMe} ligand. The presence of low-energy intraligand CT transition in these **$MoEL^{COOMe}$** compounds directly probes the electron withdrawing nature of the −COOMe substituents, and this underscores the complex electronic structure of square pyramidal bis(ene–1,2–dithiolate)-Mo^{IV} complexes that possess extended dithiolene conjugation.

†Electronic supplementary information (ESI) available: resonance Raman spectra (Figures S1–S3). CIF files. Full Gaussian03 reference.

Correspondence to: Hideki Sugimoto, sugimoto@mls.eng.osaka-u.ac.jp; Shinobu Itoh, shinobu@mls.eng.osaka-u.ac.jp; Martin L. Kirk, mkirk@unm.edu.

Introduction

Compounds with metal–ligand multiple bonds, M=E or Mo≡E (M = metal and E = element), function as key components of industrial and biological catalysts.[1] The recent structural characterisation of some mononuclear pyranopterin molybdenum enzymes has resulted in increased interest in the study of multiply bonded MoO, MoS, and MoSe units in the coordination chemistry of molybdenum.[2] A terminal oxo donor, possessing a formal triple bond, is found in many forms of pyranopterin molybdenum enzymes, which include the molybdenum hydroxylases of the xanthine oxidase enzyme family and the molybdenum oxotransferases that belong to the sulfite oxidase and DMSO reductase enzyme families.[2] In contrast to these terminal Mo-oxo bonds, a terminal sulfido donor with a reduced Mo-$S_{sulfido}$ bond order is found oriented *cis* to the apical oxo ligand in the xanthine oxidase family.[3] Also a terminal sulfido donor is included in the reduced formate dehydrogenase of molybdenum enzymes.[4] Recently, Dobbek and coworkers showed that a terminal selenide donor is found in place of the terminal sulfido present in xanthine oxidase and nicotinic acid hydroxylase.[5] Although a large number of monomeric molybdenum coordination compounds possess terminal oxo ligands, notably fewer that possess terminal sulfido ligands have been prepared and their reactivities and spectroscopic properties explored.[6,7] Even fewer studies have examined the geometric and electronic structure of molybdenum complexes that possess terminal selenido coordination due to the difficulty in synthesising MoSe complexes.[7,8,9] Additionally, there is a paucity of comparative studies on MoO, MoS and MoSe compounds that have been synthesised using the same or similar supporting ligands. The dearth of such compounds has limited our ability to make detailed geometric-electronic structure correlations as a function of the MoE unit, and this has provided the impetus for the synthesis of new monomeric compounds that possess terminal sulfido and selenido coordination.

Over a decade ago, Cotton and coworkers synthesised a series of six–coordinate distorted octahedral *trans*–$Mo^{IV}E_2(P\text{-}P)_2$ complexes (E = O, S, Se, and P-P = 1,2-bis(diphenylphosphino)ethylene or its ethane derivative (Fig. 1)).[10] Cummins and coworkers also reported a series of four coordinate distorted tetrahedral $Mo^{V}E$ complexes with an identical coligand in $Mo^{V}E(N(R)Ar)_3$ (E = O, S, Se; R = $C(CD_3)_2CH_3$, Ar = 3,5-$C_6H_3Me_2$) (Fig. 1).[11] However, no series of five–coordinate MoO, MoS, and MoSe complexes exist that possess identical supporting ligands. Furthermore, the P-P and N(R)Ar supporting ligands in the earlier studies did not possess electron withdrawing groups (EWGs) or electron donating groups (EDGs) that would allow for a systematic study of substituent effects on the electronic structure, spectroscopy and reactivities of the complexes. A classic series of $Mo^{IV/V/VI}$ S complexes, $[\{HB(R_2pz)_3\}MoS(L)_m]^{n-}$ (hydrotris(3,5-dialkylpyrazol-1-yl)borate, L = mono- or di-dentate ligands), has been prepared by Young and Enemark using sterically demanding tridentate ligands as models for Mo-sulfido centres in pyranopterin molybdenum enzymes.[12–17] This series of compounds has allowed for very meaningful systematic investigations of their geometric structures, spectroscopic properties, and reactivities by modifying both the alkyl groups, R, and the mono- and bidentate ligands, L. However, no corresponding MoSe derivatives have been reported to date.

Recently, we reported the first series of multiply bonded square pyramidal MoE (E = O, S, Se) complexes possessing an identical supporting ligand, $[Mo^{IV}E(L^{C4H8})_2]^{2-}$ (L^{C4H8} = cyclohexene-1,2-dithiolate).[18–20] These complexes make possible detailed investigations regarding the effects of the MoE unit on the structure, spectroscopy and reactivity of the complexes. Regarding the square pyramidal structure, the active sites of reduced (i.e. Mo(IV)) formate dehydrogenase and arsenite oxidase adopt similar square pyramidal bis(pyranopterin-dithiolene)-$Mo^{IV}S$ and -$Mo^{IV}O$ structures, respectively,[4,21] This has stimulated our interest in extending the $[Mo^{IV}$ Se(ene-1,2-dithiolate$)_2]^{2-}$ family to include

the ene-1,2-dithiolates, 1,2-diphenyl-1,2-dithiolate (L^{Ph}) and 1,2-dicarbomethoxyethylene-1,2-dithiolate (L^{COOMe}), allowing us to probe MoE bonding as a function of dithiolene electronic structure.

In this manuscript, we describe the synthesis and X-ray structures of $(Et_4N)_2[Mo^{IV}S(L^{Ph})_2]$ (**MoSL^{Ph}**), $(Et_4N)_2[Mo^{IV}S(L^{COOMe})_2]$ (**MoSL^{COOMe}**), as well as their selenido derivatives, $(Et_4N)_2[Mo^{IV}Se(L^{Ph})_2]$ (**MoSeL^{Ph}**) and $(Et_4N)_2[Mo^{IV}Se(L^{COOMe})_2]$ (**MoSeL^{COOMe}**) (see Fig. 2). These new molecules now complete set of $[MoEL_2]^{2-}$ (E = O, S, Se; L = L^{C4H8}, L^{Ph}, L^{COOMe}) compounds that allow the development of detailed electronic and geometric structure correlations as a function of the terminal E ligand, and this provides a means for evaluating the effects of dithiolene substituents on the structure and spectroscopic properties of these compounds. A long these lines, we have performed a detailed electronic absorption, resonance Raman and computational investigation of the $MoEL^{COOMe}$ (E = O, S, Se) series in order to understand the nature of their low energy ligand-field and charge transfer excitations and to develop a basic electronic structure description of the complexes as a function of the apical E donor.

Experimental section

General

All reagents and solvents were used as received unless otherwise noted. All reactions were carried out under a dinitrogen atmosphere using standard Schlenk techniques. Complexes of **MoOL^{C4H8}**,[18] **MoSL^{C4H8}**,[19] **MoSeL^{C4H8}**,[20] **MoOL^{Ph}**,[22] **MoOL^{COOMe}**,[23] $[Mo(CO)_2(L^{Ph})]$[24] and $(Et_4N)[Mo^{IV}(OSitBuPh_2)(L^{COOMe})_2]$ (**Mo(OSitBuPh$_2$)L^{COOMe}**)[25] were prepared by following established literature procedures.

Synthesis and characterization of complexes

$(Et_4N)_2[Mo^{IV}S(L^{Ph})_2]$ (MoSL^{Ph})—To an acetonitrile suspension containing $[Mo(CO)_2(L^{Ph})_2]$ (46 mg, 0.072 mmol), an acetonitrile suspension containing Na_2S (52 mg, 0.67 mmol) was added. After stirring for 3 hours, Et_4NCl (24 mg, 0.15 mmol) was added to the suspension. Excess Na_2S was removed by filtration and the filtrate was concentrated to dryness. The obtained green solid was dissolved in minimum volume of DMSO and diffusion of ether to the solution gave green-brown crystals of **MoSL^{Ph}**. The crystals were collected by filtration and dried under reduced pressure. Yield 44 mg (70%). Anal. Calcd for $C_{44}H_{60}MoN_2S_5$ • DMSO (mol wt. 951.38): C, 58.07; H, 6.99; N, 2.94. Found: C, 57.82; H, 6.65; N; 2.75. ^{1}H NMR (CD_3CN): δ 7.24-6.92 (m, 20H), 3.09 (q, 16H), 2.53 (s, 6H), 1.08 (t, 24H). UV-vis spectrum (CH_3CN): λ_{max} = 258 (ε = 37000), 321 (29600), 385 (13000), 450 (sh, 4660), 569 (1370), 699 nm (1240 M^{-1} cm^{-1}). ESI-MS (CH_3CN): *m*/*z* = 357 $[M]^{2-}$. CV (0.1 V s^{-1}, CH_3CN): $E_{1/2}$ (rev.) = −0.43 V vs. SCE. IR (KBr): ν 486 (s), 691 (s), 723 (s), 759 (m), 836 (s), 870 (s), 997 (m), 1026 (s), 1077 (w), 1108 (vs), 1236 (vs), 1438 (vs), 1484 (s), 1586 (w), 1707 (s), 1716 cm^{-1} (s).

$(Et_4N)_2[Mo^{IV}Se(L^{Ph})_2]$ (MoSeL^{Ph})—This complex was synthesised using the same procedure as **MoSL^{Ph}**, except Na_2Se (27 mg, 0.22 mmol) was used instead of Na_2S. Recrystallization from DMSO/ether gave a microcrystalline powder, which was collected by filtration and dried in dinitrogen. Yield: 24 mg (34%). Anal. Calcd for $C_{44}H_{60}MoN_2S_4Se$ • DMSO (mol wt. 998.25): C, 55.35; H, 6.66; N, 2.81. Found: C, 55.38; H, 6.65; N; 2.96. ^{1}H NMR (CD_3CN): δ 7.24-6.91 (m, 20H) 3.09 (q, 16H), 2.53 (s, 6H), 1.08 (t, 24H). UV-vis spectrum (CH_3CN): λ_{max} = 294 (ε = 33200), 328 (32300), 370 (sh, 14900), 414 (12000), 480 (sh, 3850), 588 (sh, 830), 705 nm (620 $M^{1-}cm^{-1}$). ESI–MS (CH_3CN): *m*/*z* = 792 $\{[M]^{2-} + Et_4N^+\}^-$. CV (0.1 V s^{-1}, CH_3CN): $E_{1/2}$(rev.) = −0.45 V vs. SCE. IR (KBr): ν 784

(m), 807 (m), 909 (s), 999 (m), 1017 (m), 1055 (m), 1152 (m), 1172 (m), 1234 (vs), 1325 (m), 1394 (s), 1431 (m), 1454 (m), 1483 (s), 1528 (s), 1696 (s), 1711 cm^{-1} (s).

$(Et_4N)_2[Mo^{IV}S(L^{COOMe})_2]$ ($MoSL^{COOMe}$)—To 10 mL of an acetonitrile solution of **$Mo(OSitBuPh_2)L^{COOMe}$** (124 mg, 0.14 mmol), 1.5 mL of an acetonitrile solution of Et_4NSH (25 mg, 0.15 mmol) was added. The resultant brown solution was concentrated to ~1 mL. A brown powder was precipitated by addition of diethyl ether to the solution, and this was collected by filtration, washed with THF/acetone, and dried in vacuo. To 3 mL of an acetonitrile solution of the brown powder, $^tBuPh_2SiCl$ (14 mL, 0.065 mmol) was added, and the solution was stirred for 5 minutes and then concentrated to 1 mL. Addition of 6 mL of THF to the solution yielded a brown powder, which was collected by filtration and washed with THF/acetone. Yield: 50.5 mg (45%). Anal. Calcd for $C_{28}H_{52}MoN_2O_8S_5$ (mol wt. 801.00): C, 41.99; H, 6.54; N, 3.50. Found: C, 41.94; H, 6.55; N; 3.53. ^1H NMR (CD_3CN, 25 °C): δ 3.725 (s, 12H), 3.09 (q, 16H), 1.08 (t, 24H). UV-vis spectrum (CH_3CN): λ_{max} = 365 (ε = 8110), 429 (2020), 505 (sh, 370), 711 nm (62 M^{-1} cm^{-1}). ESI-MS (CH_3CN): *m*/*z* = 672 $\{[M]^{2-} + Et_4N^+\}^-$. CV (CH_3CN): E^{pa}(irrev.) = −0.12 V vs. SCE. IR (KBr): ν 495 (s), 678 (w), 753 (w), 782 (m), 1014 (m), 1068 (w), 1172 (m), 1227 (vs), 1393 (m), 1433 (m), 1456 (w), 1478 (s), 1525 (s), 1684 (s), 1718 cm^{-1} (s).

$(Et_4N)_2[Mo^{IV}Se(L^{COOMe})_2]$ ($MoSeL^{COOMe}$)—To an acetonitrile solution (4 mL) containing **$Mo(OSi^tBuPh_2)L^{COOMe}$** (153 mg, 0.17 mmol), an acetonitrile suspension (1 mL) containing Na_2Se (51 mg, 0.041 mmol) was added. After stirring this suspension for 20 hours, an acetonitrile solution (1 mL) of Et_4NCl (28 mg, 0.17 mmol) was added to the reaction mixture. Undissolved Na_2Se was removed by filtration and the brown filtrate was concentrated to ca. 1 mL. A brown powder was precipitated by addition of diethyl ether to the solution, which was collected by filtration, washed with THF/acetone, and dried in dinitrogen. To an acetonitrile solution (6 mL) of the brown powder, $^tBuPh_2SiCl$ (31 mL, 0.14 mmol) was added. After stirring the solution for 5 min, the solution was concentrated to 1 mL. Addition of 12 mL of THF to the solution gave a brown powder, which was collected by filtration, washed with THF/acetone, and dried in dinitrogen. Yield: 42 mg (29%). Anal. Calcd for $C_{28}H_{52}MoN_2O_8S_4Se$ (mol wt. 847.89): C, 39.66; H, 6.18; N, 3.30. Found: C, 39.53; H, 6.13; N; 3.46. ^1H NMR (CD_3CN, 25°C): δ 3.725 (s, 12 H), 3.09 (q, 16H), 1.08 (t, 24H). UV-vis spectrum (CH_3CN): λ_{max} = 376 (ε = 8440), 458 (2020), 575 (sh, 280), 740 nm (42 M^{-1} cm^{-1}). ESI–MS (CH_3CN): *m*/*z* = 719 $\{[M]^{2-}+ Et_4N^+\}^-$. CV (CH_3CN): E^{pa} (irrev.) = −0.12 V vs. SCE. IR (KBr): ν 675 (w), 780 (m), 1013 (m), 1067 (w), 1171 (m), 1225 (vs), 1393 (m), 1432 (m), 1455 (w), 1478 (s), 1684 (s), 1718 cm^{-1} (vs).

Physical measurements

FT–IR spectra were recorded with a Perkin–Elmer Spectrum One spectrometer. Resonance Raman spectra were taken on a Jasco NRD–1000 instrument using an Ar^+ ion laser with excitation at 488 nm. Solid state resonance Raman (rR) spectra and associated rR excitation profiles were collected using a system comprised of an PI/Acton SpectraPro SP-2556 500 mm focal length imaging spectrograph with a triple grating turret and a PI/Acton Spec-10:100B back-illuminated 1340 × 100 pixel digital CCD spectroscopy system with a cryogenically cooled camera head. A Coherent Innova Ar^+ ion laser was the excitation source. Samples were mixed with either NaCl or a $NaCl/Na_2SO_4$ mixture with Na_2SO_4 as an internal calibrant. ^1H NMR spectra were recorded with a JEOL Lambda 300, and TMS signal was adjusted to 0 ppm. ^{77}Se-NMR spectra were recorded on a JEOL FT-NMR Lambda 300WB spectrometer. $(CH_3)_2Se$ was used as an internal standard. ESI–mass spectra were measured with a JEOL JMS-700S. Routine UV-vis spectra were recorded on a HP-8453 or Shimazu-UV 2550 spectrometer. Additional solution electronic absorption spectra were collected using a Hitachi U-3501 UV-Vis-NIR dual-beam spectrophotometer

capable of scanning a wavelength region between 185 and 3200 nm. Spectral samples were dissolved in dry, degassed acetonitrile, and the electronic absorption spectra were measured in a 1 cm pathlength, 100 mL, black-masked, quartz cuvette (Starna Cells, Inc.) equipped with a Teflon stopper. All electronic absorption spectra were performed at room temperature and repeated at regular time intervals to ensure the structural stability and integrity of the complex in solution.

Electrochemistry—Cyclic voltammetric measurements were performed under dinitrogen with a Hokuto Denko HZ-3000 potentiostat. A set of a glassy-carbon working electrode (circular, 3 mm diameter), a SCE reference electrode, and a platinum counter electrode was employed in these experiments.

X-ray crystallography—Single crystals of **MoSL^{Ph}•CH$_3$CN** were obtained by diffusion of diethyl ether into an acetonitrile solution of **MoSL^{Ph}**. Single crystals of **MoSeL^{Ph}•DMSO** were obtained by diffusion of diethyl ether into a DMSO solution of **MoSeL^{Ph}**. Single crystals of **MoSL^{COOMe}** and **MoSeL^{COOMe}** were obtained by diffusion of diethyl ether into each acetonitrile solution. Single crystals of **MoOL^{Ph}** were obtained by recrystallization from DMSO/diethylether. Each single crystal obtained, except for **MoOL^{Ph}**, was mounted on a glass fiber, and all X-ray data were collected at −173 °C on a Rigaku CCD diffractometer with monochromatic Mo-Kα radiation. A single crystal of **MoOL^{Ph}** was mounted on a glass fiber, and all measurements were made on a Rigaku RAXIS RAPID imaging plate area detector with graphite monochromated Mo-Kα radiation. The structures were solved by direct methods[26] and expanded using DIRDIF 99.[27] The non–hydrogen atoms were refined anisotropically by full–matrix least squares on F^2. The hydrogen atoms were attached at idealized positions on carbon atoms and were not refined. All structures in the final stages of refinement showed no movement in the atom positions. The calculations were performed using Single–Crystal Structure Analysis Software, version 3.8.[28] Crystallographic parameters are summarised in Table 1.

Electronic structure calculations—Electronic structure and vibrational frequency calculations were performed at the density functional level of theory using the Gaussian 03W software package.[29] All calculations employed the B3LYP hybrid functional and used a LANL2DZ basis set with an effective core potential for Mo. A 6-31G* basis set was used for all light atoms. Input files were prepared using the molecule builder function in the Gaussview software package. The results of these calculations were further analyzed using the program AOMix. Electron density difference maps (EDDMs) were constructed using the GaussSum suite of programs.

Results and discussion

Preparation and characterisation of Mo^{IV}S/Mo^{IV}Se complexes with L^{Ph} and L^{COOMe}

The first series of the square pyramidal bis(ene-1,2-dithiolate)Mo^{IV}E (E = O, S, Se) complexes, [Mo^{IV}E(L^{C4H8})$_2$]$^{2-}$ (**MoEL^{C4H8}**), were synthesised from Mo(CO)$_2$(L^{C4H8})$_2$ and 2 equivalent of hydroxide ion (Et$_4$NOH), 1 equivalent of sulfido ion (Na$_2$S) or 1 equivalent of selenido ion (Na$_2$Se) in dry CH$_3$CN.[18,19,20] In a similar manner, **MoSL^{Ph}** and **MoSeL^{Ph}** were synthesised. These two complexes, along with **MoOL^{Ph}**, complete the second series of Mo^{IV}E complexes including an identical ene-1,2-dithiolate ligand. The elemental analysis and negative-ion ESI-MS data for **MoSL^{Ph}** and **MoSeL^{Ph}** were consistent with the corresponding molecular formulas. For the synthesis of the Mo^{IV}S and Mo^{IV}Se species with L^{dmed}, **Mo(OSi^{t}BuPh$_2$)L^{COOMe}** was employed. When the compound was treated with one equivalent of EtN$_4$SH in acetonitrile, a mixture of two complexes was obtained. The negative ESI-MS of the acetonitrile solution containing

Mo(OSi^{t}BuPh$_2$)L^{COOMe} and Et_4NSH in a 1: 1 ratio showed two peak clusters at *m*/*z* = 656 and 672 in ca. 1: 1 ratio in intensity (Fig. 3), of which one peak cluster at *m*/*z* = 656 corresponded to the mono-oxo molybdenum complex **MoOL^{COOMe}** ($[M^{2-} + Et_4N^+]^-$), and another one at *m*/*z* = 672 was attributed to the mono–sulfido molybdenum complex **MoSL^{COOMe}** ($[M^{2-} + Et_4N^+]^-$). The ^{1}H NMR spectrum of an acetonitrile–d_3 solution containing equimolar amount of **Mo(OSi^{t}BuPh$_2$)L^{COOMe}** and EtN_4SH exhibited two singlets at 3.685 and 3.725 ppm in a 1: 1 integrate ratio. The former chemical shift was identical to that of the ^{1}H NMR signal for −COOMe groups of the **MoOL^{COOMe}** reported in the literature.[23] The IR spectrum of a powder precipitated from the solution showed strong absorption bands at 911 and 495 cm^{-1} assignable to ν(MoO) and ν(MoS) stretchings, respectively. Collectively, **Mo(OSi^{t}BuPh$_2$)L^{COOMe}** was revealed to change to the MoO and MoS compounds upon treatment with SH^-. The MoS species was purified by washing the mixture with THF containing ^{t}BuPh$_2$SiCl since **Mo(OSi^{t}BuPh$_2$)L^{COOMe}** formed again here is soluble in THF. Similarly, **MoSeL^{COOMe}** was synthesised from **Mo(OSi^{t}BuPh$_2$)L^{COOMe}** and Na_2Se in CH_3CN. Monoselenido molybdenum(IV) complexes are extremely rare and $[Mo^{IV}Se(Se_4)_2]^{2-}$, [30] is the only example of such species besides the series reported in this paper.

Crystal structures of MoS and MoSe complexes of L^{Ph} and L^{COOMe}

The crystal structures of the anionic parts of **MoSL^{Ph}** and **MoSL^{COOMe}** are shown in Figs. 4 and 5, respectively, and the selected bond distances and angles are listed in Table 2 together with those of **MoSL^{C4H8}**. The Mo1 atom of **MoSL^{Ph}** is coordinated by a terminal sulfido, S5, and four sulfur atoms, S1–S4 of two L^{Ph}. The S1, S2, S3 and S4 atoms are almost coplanar and the four bond angles, S5-Mo1-S1 (110.20(3) °), -S2 (112.08(3) °), -S3 (106.16(3) °) and -S4 (110.19(3) °) are found to be very similar. Additionally, the S1-Mo1-S3 bond angle (143.64(3) °) is very similar to the S2-Mo1-S4 (137.71(3) °) angle. Taken together, these observations indicate that each Mo1 atom possesses a distorted square pyramidal geometry as commonly found in the Mo(IV) complexes, [MoS(didentate ligand)$_2$]$^{2-}$, (bidentate ligand = S_4,[23] CS_4,[31] L^{C4H8},[18] $S_2C_2Me_2$[32]), [MoS(bdt)(S_4)]$^{2-}$,[33] and [MoS(bdtCl$_2$)(S_4)]$^{2-}$.[33] The Mo1 atom of **MoSL^{COOMe}** also adopts a similar distorted square pyramidal geometry as **MoSL^{Ph}**, and this is reflected by the S5-Mo1-S (L^{COOMe}) and S1-Mo1-S3 and S2-Mo1-S4 bond angles. With respect to the dimensions of L^{Ph} and L^{COOMe}, the four C-S bond lengths of L^{Ph} (1.766(3) – 1.789(3) Å) and the three C-S bonds (1.748(6) – 1.774(4) Å), except for the C1-S1 bond (1.735(5) Å) of L^{COOMe}, are in the typical range of C-S single bonds. The somewhat shorter L^{COOMe} S1-C1 bond length may be ascribed to the mesomeric effect of the −COOMe ester group attached on S2 atom of **MoSL^{COOMe}**, as suggested by the small 6.43(6) ° dihedral angle between the −COOMe and S1-C1-C2-S2 planes. As comparison, other three dihedral angles between −COOMe and S1-C1-C2-S2 or S3-C3-C4-S4 planes of L^{COOMe} are close to 90 °. The respective C1-C2 and C3-C4 bond lengths of **MoSL^{Ph}** (1.355(5) and 1.360(5) Å) and **MoSL^{COOMe}** (1.353(7) and 1.358(10) Å) suggest their double bond character. Collectively, these observations indicate that L^{Ph} and L^{COOMe} ligands of the MoS complexes have a structure of ene–1,2–dithiolate, as in the case of L^{C4H8} of **MoSL^{C4H8}**. The Mo1–S5 bond length of the three complexes with L^{Ph}, L^{COOMe} and L^{C4H8} increases in the order of **MoSL^{C4H8}** (2.167(2) Å) > **MoSL^{Ph}** (2.1592(9) Å) > **MoSL^{COOMe}** (2.1495(16) Å), indicating that the Lewis acidity of the central molybdenum(IV) ion decreases with an increase in L→Mo electron donation yielding weaker Mo≡S bonds.

The crystal structures of anionic parts of **MoSeL^{Ph}** and **MoSeL^{COOMe}** are shown in Figs. 6 and 7, respectively. The selected bond lengths and angles are indicated in Table 3 together with those of **MoSeL^{C4H8}**. The Mo1 atoms of **MoSeL^{Ph}** and **MoSeL^{COOMe}** are coordinated with one terminal selenido, Se1, and the four dithiolene sulfur atoms, S1–S4,

derived from either L^{Ph} or L^{COOMe}. The dimensions about each Mo1 atom are similar to those of the corresponding sulfido analogues except for the Mo1–Se1 bond distances, yielding an isostructural distorted square-pyramidal geometry. In **MoSeL^{Ph}**, the C–S bond lengths range from 1.768(3) to 1.789(5) Å and the C1-C2 and C3-C4 bond distances are 1.345(5) and 1.380(7) Å. These data suggest that the two L^{Ph} ligands of **MoSeL^{Ph}** are also ene-1,2-dithiolates and not dithiones.[34] The two L^{COOMe} ligands in **MoSeL^{COOMe}** also possess an ene-1,2-dithiolate structure as reflected by the C-S bond distances (1.749(6) - 1.769(4) Å) and the C1-C2 and C3-C4 bond lengths (1.345(6) and 1.338(7) Å). The Mo1-Se1 bond (2.3069(5) Å) of **MoSeL^{C4H8}** with the largest L→Mo charge donation is the longest in the Mo1-Se1 bonds of the three MoSeL complexes (see electrochemical section). All three of the Mo1-Se1 bond lengths are longer than the MoSe bond in square-pyramidal $[Mo^{IV}Se(Se_4)_2]^{2-}$ (2.270(4) Å).[30]

We report the crystal structure here and find the square-pyramidal geometry and the Mo≡O bond length to be 1.709(2) Å (Fig. 8 and Table 4) although **MoOL^{Ph}** had been synthesised previously.[22] In summary, the crystal structures presented here show that the bis(L)Mo^{IV}E series provides a set of isostructural complexes that can be used to evaluate the strength of the Mo≡E bonds as a function of L→Mo charge donation.

Electrochemical properties

Although the **MoSL** and **MoSeL** complexes exhibit a redox wave assignable to the Mo(V)/Mo(IV) couple, the reversibility of the redox wave is influenced by the nature of the dithiolene, L. The Mo(V)/Mo(IV) couple for **MoSL^{C4H8}** ($E_{1/2}$ = −0.75 V vs. SCE) is reversible on the cyclic voltammetry (CV) time scale using scan rates greater than 20 mV s^{-1}. The Mo(V)/Mo(IV) couple for **MoSeL^{C4H8}** was observed at $E_{1/2}$ = −0.74 V and was also observed to be reversible on the CV time scale under the same experimental conditions as **MoSL^{C4H8}**. However, both **MoSL^{Ph}** and **MoSeL^{Ph}** exhibited a noticeable scan rate dependent reversibility in the CV. Using scan rates greater than 300 mV s^{-1}, the Mo(V)/Mo(IV) redox process of these complexes exhibited a reversible wave at −0.43 V for **MoSL^{Ph}** and −0.45 V for **MoSeL^{Ph}**. The redox wave became irreversible at scan rates less than 300 mV s^{-1}. The dependence of scan rate on the CV of **MoSeL^{Ph}** is shown in Fig. 9. These observations indicate that the structure of the monomeric Mo(IV) species is unstable relative to one-electron oxidation processes. This instability likely results from dimerization, as both **MoSL^{C4H8}** and **MoSeL^{C4H8}** have been reported to yield dinuclear $\{[Mo^{V}(L^{C4H8})_2]_2(\mu\text{-}S/Se)_2\}^{2-}$ structures upon one-electron oxidation,[19,20] and the UV–vis spectra of solutions obtained by chemical oxidation of **MoSL^{Ph}** and **MoSeL^{Ph}** with ferrocenium hexafluorophosphate are identical to those of dimeric $\{[Mo^{V}(L^{Ph})_2]_2(\mu - S/Se)_2\}^{2-}$.[35] The **MoSL^{COOMe}** and **MoSeL^{COOMe}** complexes both exhibit an irreversible Mo(V)/Mo(IV) redox couple at E^{pa} = −0.12 and −0.12 V, respectively, even with scan rates greater than 500 mV s^{-1}, indicating rapid dimerization of a putative square pyramidal Mo(V) species to generate $\{[Mo^{V}(L^{COOMe})_2]_2(\mu - S/Se)_2\}^{2-}$. The marked scan rate dependency on the reversibility of the Mo(V)/Mo(IV) redox process for **MoSL** and **MoSeL** supports an argument that an increase in dithiolene L→Mo charge donation can stabilise the square pyramidal Mo(V) species. In the case of **MoOL**, the one-electron oxidized mononuclear Mo(V) form is stable and does not yield dinuclear $\{[Mo^{V}(L)_2]_2(\mu\text{-}O)_2\}^{2-}$ species. Therefore, the Mo(V)/Mo(IV) redox couple in the CV is reversible. The $E_{1/2}$ values for the **Mo(S/Se)L** series and the corresponding literature values for the **MoOL** series are summarised in Table 5. Here it is observed that the Mo(V)/Mo(IV) redox potential increases in the order $L^{COOMe} > L^{Ph} > L^{C4H8}$, indicating that L→Mo charge donation increases in the order of $L^{C4H8} > L^{Ph} > L^{COOMe}$. This is the expected trend based on the electronic donating/withdrawing nature of the substituents on the dithiolene, L. In square pyramidal bis(dithiolene)$Mo^{IV, V, VI}$ complexes that possess an apical multiply bonded ligand E, the

Mo redox orbital is Mo(d_{x2-y2}) (*see* Table 8). This redox orbital is oriented orthogonal to the Mo≡E bond with the principal lobes bisecting all four Mo-S bonds. In the C_{4v} high-symmetry limit, the Mo(d_{x2-y2}) orbital is non-bonding with respect to the apical E ligand. As a result, the nature of the Mo≡E bond should not have a dominant influence on the redox potential of a given **MoEL** complex (E = O, S, Se) at parity of the equatorial ligands. We observe that the redox potentials for the L^{Ph} and L^{C4H8} compounds as a function of E are essentially uneffected by the nature of the E donor, with potentials that vary by only 30–50 mV across a given series. This should be compared with the much larger (i.e. ~300 mV) potential shift as a function of the dithiolene for a given terminal E donor. For the L^{COOMe} compounds, **MoOL^{COOMe}** possesses a redox potential that is 90 mV more positive than for **MoOL^{COOMe}** and **MoOL^{COOMe}**. In summary, the redox potentials of the **MoEL** series are dominated by the nature of the dithiolene, but are much less affected by the nature of the terminal E donor despite the fact that the pK_b values of O^{2-} (≪0), S^{2-} (−0.85), and Se^{2-} (~3) are significantly different.[36]

^{77}Se NMR spectra of MoSeL complexes

Given the effects of E on the redox potentials of the MoEL series at parity of L are minimal, we now turn our investigation toward the effects of L on the Mo≡E bond at parity of E. For the **MoSeL** complexes, this can conveniently be accomplished using ^{77}Se NMR spectroscopy (Fig. 10). To the best of our knowledge, MoSe(NR)([N]Ar)$_2$ (R = $C(CD_3)_2CH_3$, Ar = 3,5–$C_6H_3Me_2$) and *trans*–Mo(PMe_3)$_4$(Se)$_2$ are the only examples of terminal selenido complexes that have been probed by ^{77}Se NMR spectroscopy.[10,37] Our experiments reveal the ^{77}Se NMR resonances to shift to lower magnetic field in the order **MoSeL^{C4H8}** (1827.8) < **MoSeL^{Ph}** (1895.4) < **MoSeL^{COOMe}** (2175.4 ppm). This clearly indicates that electron withdrawing substituents on L result in an increase in Se^{2-}→ Mo(IV) charge donation, which in turn results in a less basic terminal selenide. These results are important, since they suggest that the nature of the dithiolene ligand can fine-tune the acid/base and the atom transfer reactivity of terminal MoE sites in enzymes and related systems.

Spectroscopic and electronic structure studies

Solution electronic absorption spectra for **MoSL** and **MoSeL** were collected in CH_3CN. The electronic absorption spectra of the **MoOL** series have been reported previously.[18,22,23] Inspection of the absorption spectra for **MoSL** and **MoSeL** complexes reveals that they can be divided into three sections: the first region occurs at wavelengths lower than ca. 350 nm where the complexes possesses intense absorption bands with molar extinction coefficients (ε) over ~10,000 M^{-1} cm^{-1}, the second region occurs between 350 – 600 nm and displays a well-defined band with an extinction coefficient of ca. 2000 M^{-1} cm^{-1}, and finally a third low-energy region that consists of a series of weak absorption bands. The well-defined band that appears in the second spectral region was previously tentatively assigned as an E→Mo(IV) charge transfer band, with respect to the prior spectral assignments for *trans*–Mo(E)$_2$(PMe_3)$_4$ (E= O, S, or Se) and *trans*–Mo(E)$_2$(P–P)$_2$ (E = O, S, and Se).[37,10] The solution electronic absorption spectra of **MoEL^{COOMe}** (E = O, S, Se) and **MoSeL** are shown in Fig. 11. Interestingly, the prominent band in the second spectral region is shifted progressively to lower energy in the **MoEL^{COOMe}** series as a function of the terminal chalcogen donor atoms (**MoOL^{COOMe}**, 380 nm; **MoSL^{COOMe}**, 429 nm; **MoSeL^{COOMe}**, 458 nm), and this reflects a significant degree of E wavefunction mixing with the *dithiolene* frontier orbitals, *vide infra*. Finally, this CT band shifts to higher energy with a decrease in L → Mo charge donation (E = S; 462 nm for L^{C4H8}, 450 nm for L^{Ph}, 429 nm for L^{COOMe}: E = Se; 489 nm for L^{C4H8}, 480 nm L^{Ph}, 458 nm for L^{COOMe}).

Understanding the nature of key M-L vibrations in these **MoEL** (E = O, S, Se) complexes is important in developing a greater understanding of important bonding interactions in both

synthetic model systems and the enzymes, particularly those of the DMSOR enzyme family that possesses bis-dithiolene coordination. Solid-state rR spectra for the **MoEL^{COOMe}** series are presented in Fig. S1 (Supplementary Information) and summarised in Table 6. Additionally, solution resonance Raman (rR) spectra of **MoOL**, **MoSL** and **MoSeL$^{Ph,\ COOMe}$** in CH_3CN were obtained using 488 nm excitation. The Raman data are presented in Figs. S2 and S3 (Supplementary Information) and are summarized in Table 7 for comparative purposes. We were not able to obtain a Raman spectrum for **MoSeL^{C4H8}** due to decomposition as a result of the incident laser radiation. Vibrational assignments are consistent with calculated virbrations and earlier vibrational assignments made by Spiro *et al* for **MoOL^{COOMe}**.[38]

With respect to the **MoSeL^{C4H8}** and **MoEL^{Ph}** (E = O, S, Se) solution rR spectra, neither ν(Mo≡Se) for **MoSeL^{C4H8}** or ν(C=C) for **MoEL^{Ph}** could be assigned due to spectral overlap of the intrinsic compound vibrations with modes associated with the solvent. For the **MoEL^{COOMe}** (E = O, S, Se) series, there is very good agreement between the solution and solid state spectra and this indicates the integrity and geometry of the complexes are maintained in solution. The Raman data for the **MoEL^{COOMe}** series reveal that the ν(Mo≡E) stretching frequency is shifted to lower energy according to O>S>Se, and reflect reduced mass differences within the Mo≡E unit. This is in marked contrast to the ν(C=C) and ν(M-$S_{dithiolene}$) stretching frequencies across this series which remain essentially constant. These observations indicates that E→Mo charge donation does not dominate Mo-$S_{dithiolene}$ bonding interactions or bonding interactions within the dithiolenes. However, the ν(Mo≡O/S) stretch in the **Mo(O/S)L** series does shift to lower frequency as a function of increased L→Mo charge donation, and this effect is greatest for the **MoSL** series. Specifically, this reflects the relative degree of L→Mo charge donation into the Mo(d_{xz}, d_{yz}) orbitals, which are π-antibonding with respect to the Mo≡E bonding scheme, and the amount of E character admixed into the Mo(d_{xz}, d_{yz}) orbitals. These results are also consistent with the change in Mo≡S bond length for the **MoSL** complexes (2.167(2) Å for L^{C4H8} > 2.1592(9) Å for L^{Ph} > 2.1495(16) Å for L^{COOMe}). Finally, our vibrational data indicate that electron withdrawing substituents on the dithiolene noticeably reduce the ν(C=C) stretching frequency (1593 cm^{-1} for L^{C4H8} > 1531 cm^{-1} for L^{COOMe}), and this is due to electron withdrawal from occupied frontier dithiolene orbitals that possess C=C π-bonding character.

Electronic structure calculations have been performed on the **MoEL^{COOMe}** series in order to obtain insight into the nature of the frontier molecular orbital bonding scheme and spectroscopy of these complexes. The relevant frontier molecular orbitals for **MoOL^{COOMe}** and **MoSeL^{COOMe}** are shown in Fig. 12, and the fragment orbital contributions to these MOs are listed in Table 8. The frontier molecular orbitals for **MoSL^{COOMe}** are provided in Fig. S4 since their appearance is essentially identical to those of **MoSeL^{COOMe}**. Assuming idealized C_{2v} symmetry, the HOMO-1 for these **MoEL^{COOMe}** complexes is principally a dithiolene S based MO of b_1 symmetry with a noticeable degree of apical E(p_x) character (Table 8). The E character in the HOMO-1 orbital is observed to decrease from E=Se to E=O, and this reflects the progressively higher valence ionization energy and electronegativity of the terminal E donor that is commensurate with a decrease in principle quantum number. As mentioned previously, the HOMO is the Mo(d_{x2-y2}) redox orbital of a_1 symmetry (idealized C_{2v}) and is essentially invariant across the series with ~80% Mo character and <1% terminal E character (Table 8), consistent with our vibrational and electrochemical results, *vide supra*. The LUMO and LUMO+1 for the **MoEL^{COOMe}** complexes are dithiolene based orbitals with C=C π* character. However, the LUMO also possesses some Mo(d_{yz})-E π* character which decreases appreciably (**MoOL^{COOMe}**: 2.8% O; **MoEL^{COOMe}**: 11.8% S; **MoEL^{COOMe}**: 13.6% Se; Table 8) with increasing apical ligand electronegativity. These results are interesting in that there exists a pair of low energy

acceptor orbitals with significant ligand character that lie between the filled Mo(d_{x2-y2}) HOMO and the rest of the Mo(IV) d-orbital manifold. Importantly, this provides a mechnanism for low-energy MLCT transitions in **MoEL^{COOMe}** compounds. The LUMO+2 and LUMO+3 orbitals for **MoOL^{COOMe}** are the Mo(d_{yz}) and Mo(d_{xz}) orbitals, respectively, and these also possess π antibonding interactions with the terminal oxo p_y and p_x orbitals. This orbital ordering is reversed for **Mo(S/Se)L^{COOMe}** with the Mo(d_{yz}) observed at higher energy than the Mo(d_{xz}). This results from stronger orbital mixing with the dithiolene-based LUMO, which also possesses some Mo(d_{yz})-E π* character. The LUMO+4 for **Mo(S/Se)L^{COOMe}** and the LUMO+6 for **Mo(O)L^{COOMe}** are higher energy unoccupied Mo(d_{z2}) orbitals which are σ* with the apical E donor. Due to the stronger ligand field of the terminal oxo donor, the Mo(d_{z2}) orbital is at higher energy for **Mo(O)L^{COOMe}**.[39,40] The LUMO+10 for **Mo(S/Se)L^{COOMe}** and the LUMO+9 for **Mo(O)L^{COOMe}** are the unoccupied Mo(d_{xy}) orbitals which are σ* with the equatorial dithiolene S donors. The high energy of the Mo(d_{z2}) and Mo(d_{xy}) orbitals restricts their ability to function as acceptor orbitals in low-energy LMCT transitions.

The electronic absorption spectrum for **MoOL^{COOMe}** is presented in Fig. 13a along with resonance Raman excitation profiles for the ν(Mo-$S_{dithiolene}$), ν(Mo≡O), ν(C-O + C-C), ν(C=C) and ν(C=O) vibrations. Gaussian resolution of the electronic absorption spectrum reveals the presence of four bands below ~27,000 cm^{-1}. These bands have been assigned (Table 9) based on their <Fig. 13, Table 7> relative intensities and energies, the nature of the rR excitation profiles, and via a computationally assisted approach using the results of our bonding (Fig. 13) and time dependent density functional theory calculations. From these data, we can assign bands 1 and 2 as the HOMO → LUMO and HOMO → LUMO+1 MLCT transitions. These assignments are strongly supported by the nature of the rR profile, which shows resonance enhancement of ligand ν(C-O + C-C), ν(C=C) and ν(C=O), but no resonance enhancement of ν(Mo-$S_{dithiolene}$) or ν(Mo≡O) under band 1. The fact that the ν(Mo≡O) mode is not resonantly enhanced under band 1 confirms the results of our bonding calculations which show the expected result that the Mo(d_{x2-y2}) HOMO wavefunction possesses no oxo character. Furthermore, the lack of a ν(Mo≡O) stretch indicates a minimal admixture of Mo(d_{xz}, d_{yz})-O π* character in the ligand-based LUMO and LUMO+1 orbitals. Bands 3 and 4 are assigned as HOMO-1→LUMO and HOMO-1→LUMO+1 transitions, respectively. Since the HOMO-1 is non-bonding with the Mo centre, we anticipate no enhancement of the ν(Mo-$S_{dithiolene}$) stretch and enhancement of ν(C-O + C-C), ν(C=C) and ν(C=O) vibrations and this is observed experimentally, confirming these band assignments. The nature of the HOMO-1→LUMO and HOMO-1→LUMO+1 transitions are unusual for this type of complex as they are *intraligand* transitions described by a charge transfer from the dithiolene S donors to the carbon backbone of the dithiolene ligand. A similar intraligand charge transfer transition has very recently been observed in Tp*MoO(S_2BMOQO) (BMOQO = 2-(3-butynyl-2-methyl-2-ol)quinoxaline), which possesses a donor-acceptor type dithiolene ligand.[41] The nature of the intraligand charge transfer is apparent in the electron density difference map (EDDM) constructed for the HOMO-1→LUMO+1 transition (Fig. 13, band 4). The observation of such intraligand charge transfer bands in **MoOL^{COOMe}** underscores the electron withdrawing nature of the −COOMe groups in **L^{COOMe}** dithiolenes.

The electronic absorption spectra of **MoSL^{COOMe}** and **MoSeL^{COOMe}** are presented in Figs. 13b and 13c, respectively, and their transition energies and band assignments are summarised in Table 9. Resonance Raman excitation profiles have been constructed for the ν(Mo-$S_{dithiolene}$), ν(Mo≡Se), ν(C-O + C-C), ν(C=C) and ν(C=O) vibrations of **MoSeL^{COOMe}** and these are overlayed on the absorption spectrum of **MoSeL^{COOMe}** in Fig. 13c. Gaussian resolution of the electronic absorption spectra for **MoSL^{COOMe}** and **MoSeL^{COOMe}** yield five bands at energies below ~27,000 cm^{-1}. Due to the similar spectral

features observed for **MoSL^{COOMe}** and **MoSeL^{COOMe}** we will discuss their band assignments together. Band 1 is assigned as the HOMO → LUMO ligand field transition (Mo(d_{x2-y2}) → Mo(d_{yz})) that possesses some MLCT character (Fig. 12) while band 2 is assigned as the HOMO → LUMO+2 ligand field transition (Mo(d_{x2-y2}) → Mo(d_{xz})). The small energy splitting of these bands, coupled with their similar transition energies, indicates nearly equivalent ligand field strengths for the terminal sulfido and selenido donors in **MoSL^{COOMe}** and **MoSeL^{COOMe}**. Band 3 is the first LMCT band and is primarily described as a HOMO-1 → LUMO one-electron promotion with some intraligand CT character. Both the HOMO → LUMO+1 and HOMO-1 → LUMO+2 contribute to the spectral region defined by band 4. This is supported by resonance enhancement of both the ν(Mo-$S_{dithiolene}$) and the ν(C=C) modes in **MoSeL^{COOMe}**. Interestingly, the ν(Mo≡Se) mode is only weakly resonance enhanced with excitation into band 4 and this likely results from a smaller contribution of the HOMO-1 → LUMO+2 one electron promotion to this band compared to the HOMO → LUMO+1. Large resonance enhancement of ν(C=C), ν(C=O), ν(Mo-$S_{dithiolene}$) and ν(Mo≡E) vibrational modes supports an assignment of both the HOMO-1 → LUMO+1 and HOMO-1 → LUMO+3 one-electron promotions as dominant contributors to band 5. The EDDMs for the two transitions that principally contribute to this band in **MoSeL^{COOMe}** are given in Fig. 14. Collectively, the assignments for band 5 in **MoSL^{COOMe}** and **MoSeL^{COOMe}**, and for the corresponding band 4 in **MoOL^{COOMe}** indicate that the one-electron promotions that contribute to these transitions originate from the HOMO-1 orbital, and this orbital possesses increased E character in the order O < S < Se. Therefore, the E character in the HOMO-1 orbitals contribute to the progressive shift of this band to higher energies, and this is consistent with the electronegativity and valence ionization energy of the terminal E donor.[40]

Conclusions

We have synthesised and structurally characterised new square pyramidal bis(ene-1,2-dithiolate)Mo^{IV}(S/Se) complexes with L^{C4H8}, L^{Ph} and L^{COOMe} ligands that, when coupled with the known $Mo^{IV}O$ complexes of L^{Ph} and L^{COOMe}, have enabled a systematic study of the effects of terminal chalcogenido and ene-1,2-dithiolate ligands on geometric and electronic structure. The structural data indicate that the Mo≡E bond lengths decrease according to $L^{C4H8} > L^{Ph} > L^{COOMe}$, reflecting the relative electron donating and withdrawing nature of the substituents on the dithiolene ligands. Dithiolene ligand effects on the nature of the Mo≡E bonds have been probed in our electrochemical investigations, where it was shown that the redox potential for the Mo(V)/Mo(IV) couple was shifted more positive as the dithiolene ligand L changed from L^{C4H8} to L^{Ph} to L^{COOMe}. Electrochemical, spectroscopic, and bonding calculations are consistent with a redox orbital that is dominantly Mo(d_{x2-y2}) in character and possesses no contribution from the terminal E donor. ^{77}Se NMR spectroscopy on **MoSeL** complexes showed that the ^{77}Se resonances shifted to lower magnetic field as the terminal selenido donor became less basic. Optical spectroscopic studies on the **MoEL^{COOMe}** (E = O, S, Se) series have allowed detailed band assignments to be made for all three compounds, and this has resulted in a greater understanding of their electronic structures. Specifically, it was found that certain low-energy transitions possessed considerable intraligand charge transfer character described by a substantial dithiolene S charge donation to the carbon backbone of the dithiolene ligand, underscoring the electron withdrawing nature of the −COOMe substituents in the **L^{COOMe}** dithiolenes. The Mo(d_{x2-y2}) → Mo(d_{xz}, d_{yz}) ligand field transitions were assigned for the **MoEL^{COOMe}** (E = S, Se) complexes yielding a spectroscopic t_{2g} splitting of ~14,500 cm^{-1}. This may be compared with an ~12,000 cm^{-1} Mo(d_{x2-y2}) → Mo(d_{xz}, d_{yz}) ligand field for des-oxo Mo^{IV}(ER)(dithiolene) (E = O, S, Se) complexes studied by Holm, Kirk and coworkers.[40] Finally, the origin of spectral shifts in the **MoEL^{COOMe}** (E = O, S, Se) series can be explained by 1) the much stronger ligand field exerted by the terminal oxo ligand that

results in markedly higher energy ligand field bands for **MoOL^{COOMe}**, and 2) the nature of the dithiolene-based LUMO wavefunction, which possesses increased E character and leads to lower energy HOMO→LUMO and HOMO-1→LUMO CT transitions as the apical chalcogenido electronegativity decreases.

Supplementary Material

Refer to Web version on PubMed Central for supplementary material.

Acknowledgments

This work was partly supported by a grant (Grant 22108520 to H.S.) for Scientific Research on Priority Areas "Coordination Programming" from MEXT of Japan. M.L.K. acknowledges the National Institutes of Health (GM-057378) for financial assistance.

References

1. Nugent, WA.; Mayer, JM. Metal–Ligand Mutiple Bonds. John Wiley; New York: 1988. Limberg C. Angew Chem Int Ed. 2009; 48:2270.
2. Hille R. Chem Rev. 1996; 96:2757. [PubMed: 11848841] Tunney, JM.; McMaster, L.; Garner, CD. Comprehensive Coordination Chemistry II. McCleverty, JA.; Meyer, JM., editors. Vol. 8. 2004. p. 459Burgmayer SJN. Prog Inorg Chem. 2004; 52:491.Young, CG. Encyclopedia of Inorganic Chemistry 2. King, RB., editor. Vol. 5. 2005. p. 3321
3. Okamoto K, Matsumoto K, Hille R, Eger BT, Pai EF, Nishino T. Proc Natl Acad Sci USA. 2004; 101:7931. [PubMed: 15148401] Doonan CJ, Rubie ND, Peariso K, Harris HH, Knottenbelt SZ, George GN, Young CG, Kirk ML. J Am Chem Soc. 2008; 130:55. [PubMed: 18062689]
4. Raaijimakers HCA, Romao MJ. J Biol Inorg Chem. 2006; 11:1261.
5. Wagener N, Pierik AJ, Ibdah A, Hille R, Dobbek H. Proc Natl Acad Sci USA. 2009; 106:11055. [PubMed: 19549881]
6. Holm RH. Coord Chem Rev. 1990; 100:183.Young, CG. Biomimetic Oxidations Catalyzed by Transition Metal Complexes. Meunier, B., editor. 2000. p. 415
7. Young, CG. Comprehensive Coordination Chemistry II. McCleverty, JA.; Meyer, JM., editors. Vol. 4. 2004. p. 415
8. Enemark JH, Cooney JLA, Wang J-J, Holm RH. Chem Rev. 2004; 104:1175. [PubMed: 14871153]
9. Sugimoto H, Tsukube H. Chem Soc Rev. 2008; 37:2609. [PubMed: 19020675]
10. Cotton FA, Schmid G. Inorg Chem. 1997; 36:2267. [PubMed: 11669860]
11. Johnson AR, Davis WM, Christopher C, Cummins CC, Serron S, Nolan SP, Musaev DG, Morokuma K. J Am Chem Soc. 1998; 120:2071.
12. Young CG, Wedd AG. Chem Comm (Feature Article). 1997:1251.
13. Young CG, Roberts SA, Ortega RB, Enemark JH. J Am Chem Soc. 1987; 109:2938.
14. Young CG, Gable RW, Hill JP, George GN. Eur J Inorg Chem. 2001:2227.
15. Doonan CJ, Nielsen DJ, Smith PD, White JM, George GN, Young CG. J Am Chem Soc. 2006; 128:305. [PubMed: 16390160]
16. Drew SC, Hill JP, Lane I, Hansen GR, Gable RW, Young CG. Inorg Chem. 2007; 46:2373. [PubMed: 17343374]
17. Laughlin LJ, Eagle AA, George GN, Tiekink ERT, Young CG. Inorg Chem. 2007; 46:939. [PubMed: 17257038]
18. Sugimoto H, Harihara M, Shiro M, Sugimoto K, Tanaka K, Miyake H, Tsukube H. Inorg Chem. 2005; 44:6386. [PubMed: 16124818]
19. Sugimoto H, Sakurai T, Miyake H, Tanaka K, Tsukube H. Inorg Chem. 2005; 44:6927. [PubMed: 16180851]
20. Tano H, Tajima R, Miyake H, Itoh S, Sugimoto H. Inorg Chem. 2008; 47:7465. [PubMed: 18683920]

21. Ellis PJ, Conrads T, Hille R, Kuhn P. Structure. 2001; 9:125. [PubMed: 11250197]
22. Lim BS, Holm RH. J Am Chem Soc. 2001; 123:1920. [PubMed: 11456813]
23. Coucouvanis D, Hadjikyriacou A, Toupadakis A, Koo SM, Ileperuma O, Draganjac M, Salifoglou A. Inorg Chem. 1991; 30:754.
24. Schrauzer GN, Mayweg VP, Heinrich W. J Am Chem Soc. 1966; 88:8174.
25. Sugimoto H, Tatemoto S, Suyama K, Miyake H, Mtei RP, Itoh S, Kirk ML. Inorg Chem. 2010; 49:5368. [PubMed: 20491454]
26. Burla MC, Camalli M, Carrozzini B, Cascarano GL, Giacovazzo C, Polidori G, Spagna R. J Appl Crystallogr. 2003; 36:1103.
27. Beurskens, PT.; Admiraal, G.; Beurskens, G.; Bosman, WP.; de Gelder, R.; Israel, R.; Smits, JMM. Technical Report of the Crystallography Laboratory. University of Nijmegen; The Netherlands: 1999. The DIRDIF-99 program system.
28. Crystal Structure Analysis Package. Rigaku and Rigaku/MSC; The Woodlands, TX, USA: 2000–2006.
29. Gaussian 03. R. C. G., IncPittsburgh, PA2003Inc (full reference is given in Supplementary Information).
30. O'Neal S, Kolis JW. J Am Chem Soc. 1988; 110:1971.
31. Coucouvais D, Draganjac MJ. J Am Chem Soc. 1982; 104:6820.
32. Groysman S, Holm RH. Inorg Chem. 2007; 46:4090. [PubMed: 17432849]
33. Sugimoto H, Suyama K, Sugimoto K, Miyake H, Takahashi I, Hirota S, Itoh S. Inorg Chem. 2008; 47:10150. [PubMed: 18826211]
34. The C1–C2 and C3–C4 distances are somewhat longer than those of complete C=C double bonds.
35. Lim BS, Donahue JP, Holm RH. Inorg Chem. 2000; 39:263. [PubMed: 11272534]
36. Atkins, P.; Orerton, T.; Rourke, J.; Weller, M.; Armstrong, F. Inorganic Chemistry. 4. Oxford University Express; New York: 2006.
37. Murphy VJ, Parkin G. J Am Chem Soc. 1995; 117:3522.
38. Subramanian P, Burgmayer S, Richards S, Szalai V, Spiro TG. Inorg Chem. 1990; 29:3849.
39. Inscore FE, McNaughton R, Westcott BL, Helton ME, Jones R, Dhawan IK, Enemark JH, Kirk ML. Inorg Chem. 1999; 38:1401.
40. McNaughton RL, Lim BS, Knottenbelt SZ, Holm RH, Kirk ML. J Am Chem Soc. 2008; 130:4628. [PubMed: 18341333]
41. Matz KG, Mtei RP, Leung B, Burgmayer SJN, Kirk ML. J Am Chem Soc. 2010; 132:7830. [PubMed: 20481628]

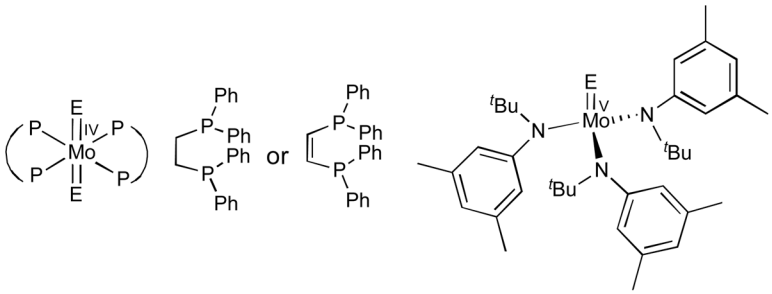

Fig. 1.
Designation and abbreviation of MoE complex structures reported previously (E = O, S, Se). ref. 10,11

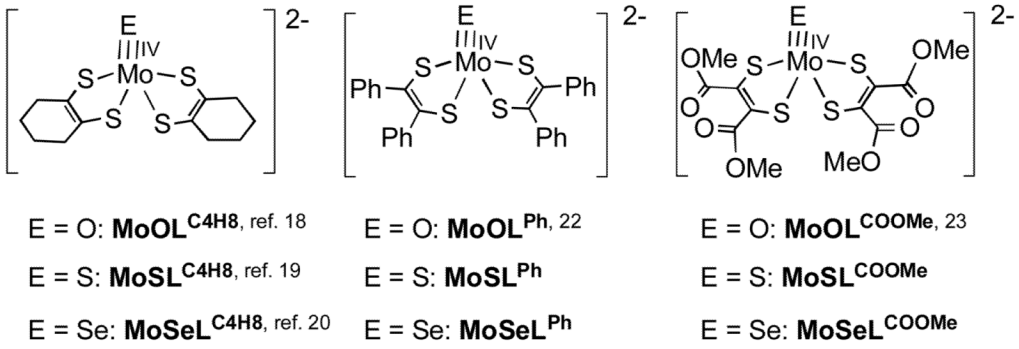

E = O: **MoOL^{C4H8}**, ref. 18 E = O: **MoOL^{Ph}**, 22 E = O: **MoOL^{COOMe}**, 23

E = S: **MoSL^{C4H8}**, ref. 19 E = S: **MoSL^{Ph}** E = S: **MoSL^{COOMe}**

E = Se: **MoSeL^{C4H8}**, ref. 20 E = Se: **MoSeL^{Ph}** E = Se: **MoSeL^{COOMe}**

Fig. 2.
Designation and abbreviation of complex structures.

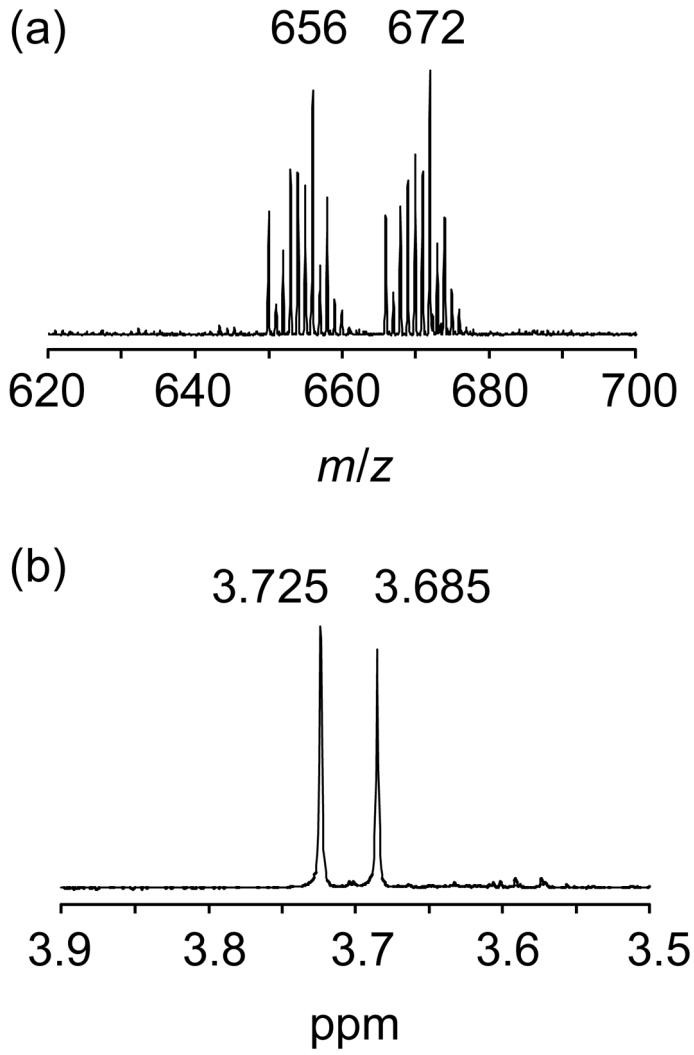

Fig. 3.
ESI mass (a) and ^{1}H NMR (b) spectra obtained by a treatment of Mo(OSi^{t}BuPh$_2$)L^{COOMe} with 1 equiv of SH^{-} in acetonitrile.

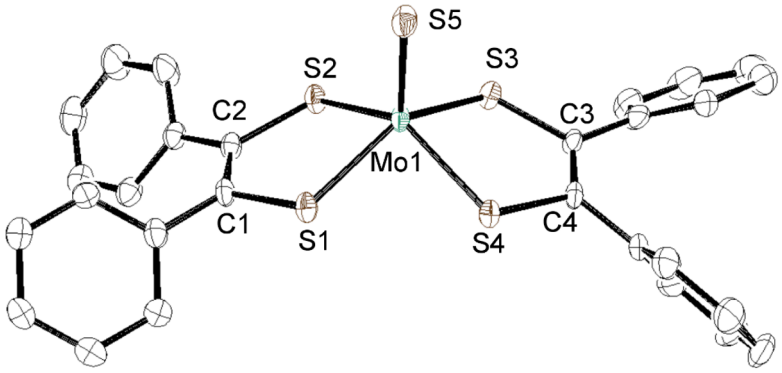

Fig. 4.

Crystal structure of the anionic part of **MoSL^{Ph} • CH$_3$CN** shown with 50% ellipsoids. The hydrogen atoms were omitted for clarity.

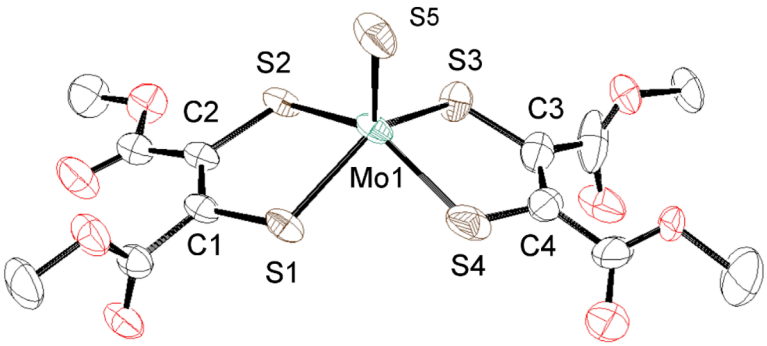

Fig. 5.
Crystal structure of the anionic part of **MoSL^{COOMe}** shown with 50% ellipsoids. The hydrogen atoms were omitted for clarity.

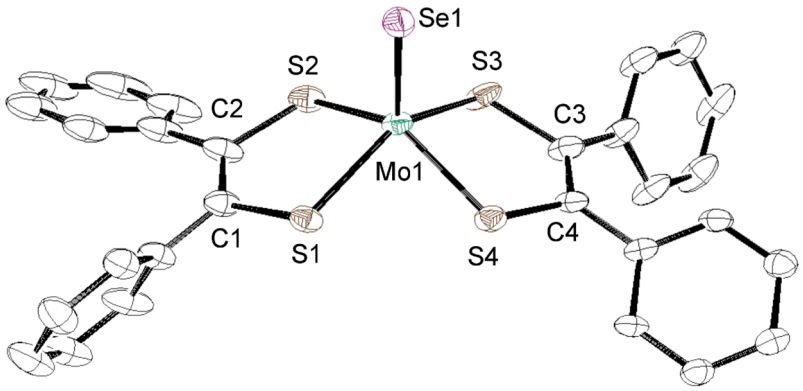

Fig. 6.

Crystal structure of the anionic part of **MoSeL^{Ph} • DMSO** shown with 50% ellipsoids. The hydrogen atoms were omitted for clarity.

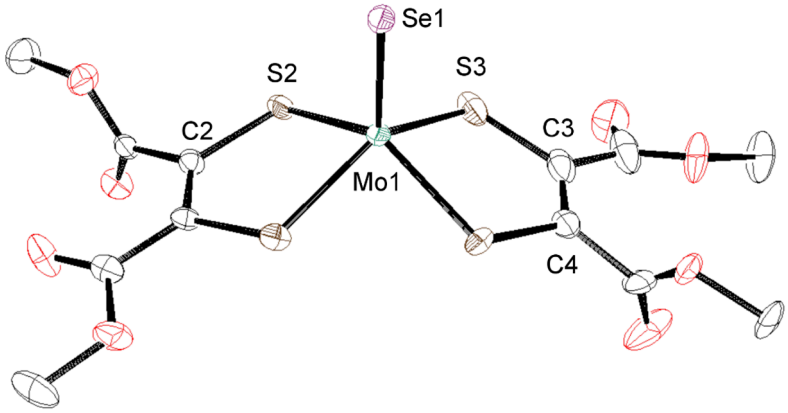

Fig. 7.
Crystal structure of the anionic part of **MoSeL^{COOMe}** shown with 50% ellipsoids. The hydrogen atoms were omitted for clarity.

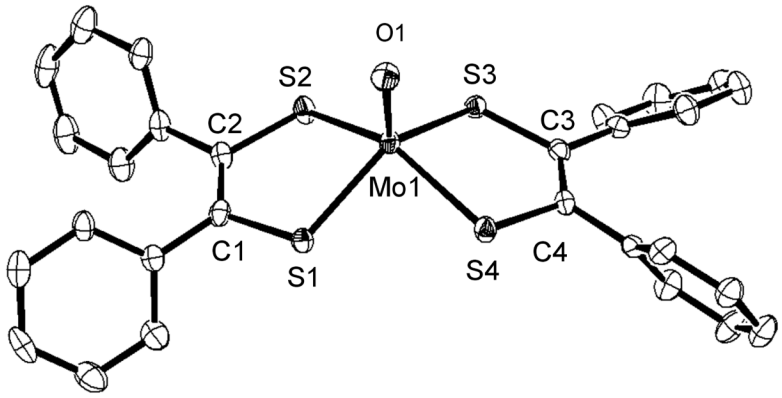

Fig. 8.
Crystal structure of the anionic part of **MoOL^{Ph}** shown with 50% ellipsoids. The hydrogen atoms were omitted for clarity.

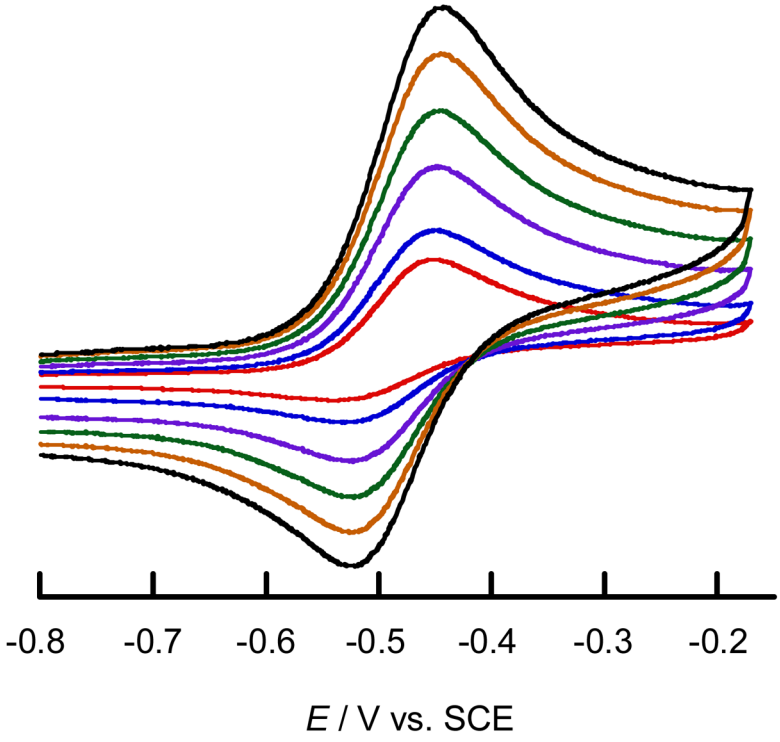

Fig. 9.

Scan rate dependent cyclic voltammogram of **MoSeL^{Ph}** in CH_3CN, 500 (black), 400 (brown), 300 (green), 200 (purple), blue (100), and 50 mV s^{-1} (red).

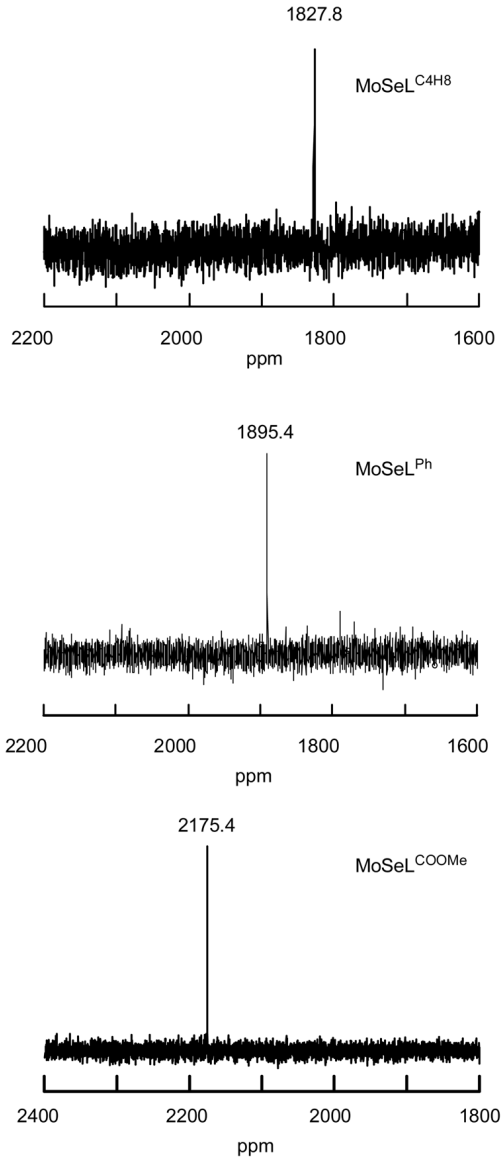

Fig. 10.
^{77}Se NMR spectra of **MoSeL^{C4H8}** (above), **MoSeL^{Ph}** (middle), and **MoSeL^{COOMe}** (bottom) in $(CD_3)_2SO$.

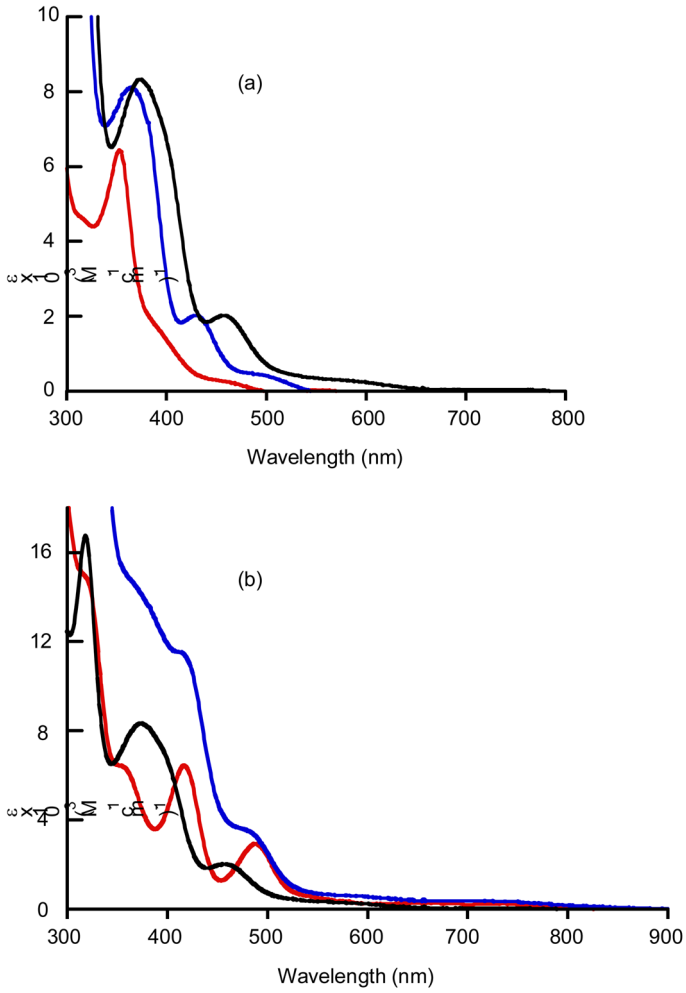

Fig. 11.

Absorption spectra in visible region in CH_3CN: (a) **MoEL**$^{\mathbf{COOMe}}$ (O (red), S (blue), and Se (black)), (b) **MoSeL** (L^{C4H8} (red), L^{Ph} (blue), and L^{COOMe} (black)).

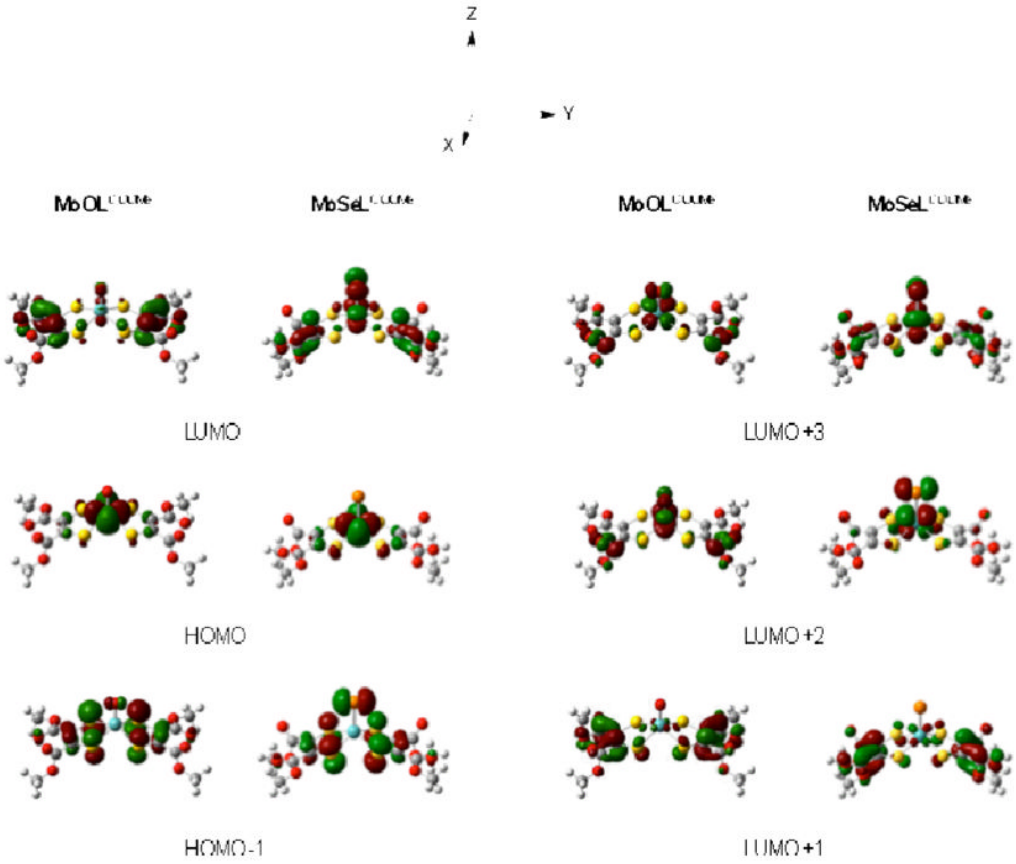

Fig. 12.
Frontier Kohn-Sham orbitals for **MoSeL^{COOMe}**. The corresponding orbitals for Mo(O/S)L^{COOMe} are very similar with important differences detailed in the text.

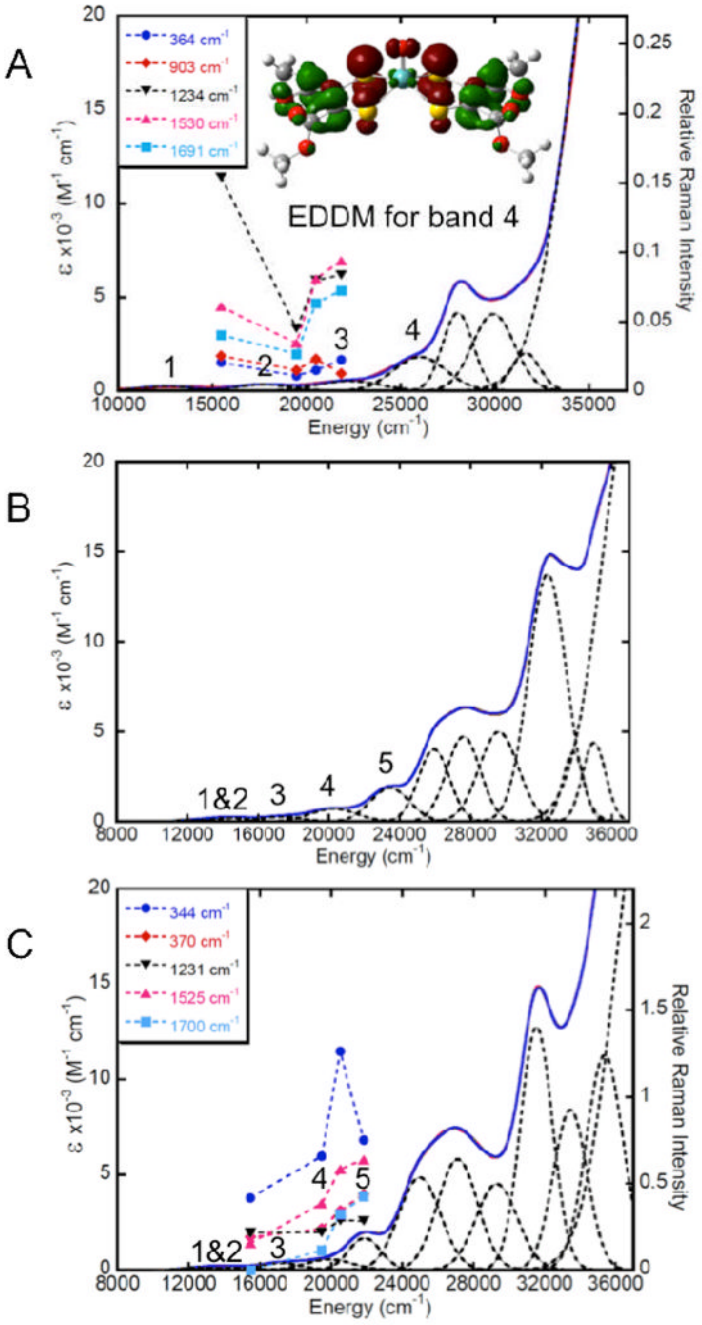

Fig. 13.

Gaussian resolved solution electronic absorption spectra for **MoOL**$^{\mathbf{COOMe}}$ (A), **MoSL**$^{\mathbf{COOMe}}$ (B), and **MoSeL**$^{\mathbf{COOMe}}$ (C). Resonance Raman excitation profiles for **MoOL**$^{\mathbf{COOMe}}$ and MoSeL$^{\mathrm{COOMe}}$ are overlayed on their respective absorption spectra. An electron density difference map that details the nature of the intraligand transition (HOMO-1→LUMO+1) in **MoOL**$^{\mathbf{COOMe}}$ (red: electron density loss in transition, green: electron density gain in transition) is presented in A (inset).

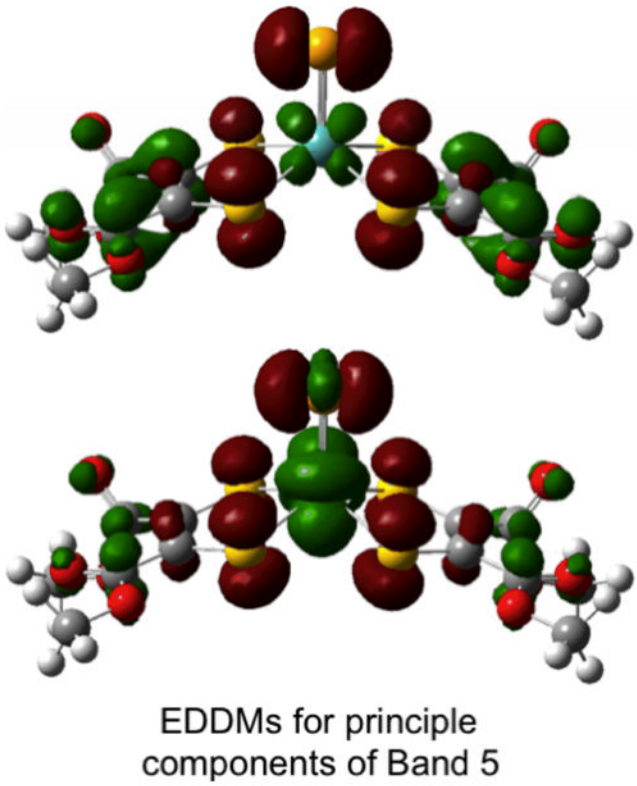

Fig. 14.

Electron density difference maps for the two transitions that comprise band 5 that detail the nature of the intraligand (HOMO-1→LUMO+1) and LMCT (HOMO-1→LUMO+3) one-electron promotions in **MoSeL^{COOMe}** (red: electron density loss in transition, green: electron density gain in transition) is presented in A (inset). Notice the increased in the Se→Mo charge transfer contribution to this transition relative to **MoOL^{COOMe}** (Figure 13A inset).

Table 1

Crystallographic Data for **MoSL^{Ph}•CH$_3$CN**, **MoSeL^{Ph}•DMSO**, **MoSL^{COOMe}**, **MoSeL^{COOMe}** and **MoOL^{Ph}**

	MoSL^{Ph}•CH$_3$CN	**MoSeL^{Ph}•DMSO**	**MoSL^{COOMe}**	**MoSeL^{COOMe}**	**MoOL^{Ph}**
formula	$C_{46}H_{63}MoN_3S_5$	$C_{46}H_{66}MoN_2OS_5Se$	$C_{28}H_{52}MoN_2O_8S_5$	$C_{28}H_{52}MoN_2O_8S_4Se$	$C_{44}H_{60}MoN_2OS_4$
fw	914.26	998.24	800.97	847.87	857.15
cryst system	orthorhombic	monoclinic	orthorhombic	orthorhombic	monoclinic
space group	$P2_12_12_1$	$P2_1/c$	*Pbca*	*Pbca*	$P2_1$
a, Å	19.519(4)	10.628(2)	12.8056(5)	12.7676(7)	14.733(9)
b, Å	20.011(4)	19.035(4)	18.2219(8)	18.3036(10)	8.778(5)
c, Å	11.887(2)	24.634(5)	31.5759(15)	31.9341(17)	17.409(11)
β, deg	90	107.256(2)	90	90	104.966(10)
V, Å^3	4643.1(15)	4759.2(16)	7368.0(6)	7462.8(7)	2175.0(23)
Z	4	4	8	8	2
ρ, g cm^{-3}	1.308	1.393	1.444	1.509	1.309
μ, mm^{-1}	0.541	1.295	0.685	1.596	0.528
data	13116	37472	54114	56065	21205
unique data	11310	10659	7969	8435	9877
*R*1[a]	0.0510	0.0568	0.0712	0.0566	0.0443
*wR*2 (F^2)[b]	0.1261	0.1686	0.1457	0.1689	0.1097
GOF	0.953	0.962	1.053	1.029	1.028

[a] $R1 = \Sigma(|F_O| - |F_C|)/\Sigma|F_O|$.

[b] $wR2 = \{\Sigma(w(Fo^2 - Fc^2)^2)/\Sigma w(F_O^2)^2\}^{1/2}$.

Table 2

Selected Bond Distances (A) and Angles (deg) of **MoSL^{Ph}•CH$_3$CN**, **MoSL^{COOMe}** and **MoSL^{CC4H8}**

	MoSL^{Ph}•CH$_3$CN	**MoSL^{COOMe}**	**MoSL$^{C4H8, a}$**
Mo1–S5	2.1592(9)	2.1495(16)	2.167(2)
Mo1–S1	2.3577(8)	2.3740(13)	2.369(2)
Mo1–S2	2.3675(8)	2.3696(14)	2.364(2)
Mo1–S3	2.3455(9)	2.3623(13)	2.382(2)
Mo1–S4	2.3656(8)	2.3601(18)	2.369(2)
S1–C1	1.781(3)	1.735(5)	1.775(8)
S2–C2	1.789(3)	1.774(4)	1.75(1)
S3–C3	1.766(3)	1.748(6)	1.753(8)
S4–C4	1.779(3)	1.770(8)	1.772(9)
C1–C2	1.355(5)	1.353(7)	1.33(1)
C3–C4	1.360(5)	1.358(10)	1.35(1)
Mo1–4S plane	0.7981(5)	0.7968(9)	0.79(1)
S5–Mo1–S1	110.20(3)	108.17(5)	106.46(9)
S5–Mo1–S2	112.08(3)	109.36(6)	110.39(9)
S5–Mo1–S3	106.16(3)	111.53(5	109.12(9)
S5–Mo1–S4	110.19(3)	109.56(6)	111.82(9)
S1-Mo1-S2	81.86(2)	83.07(4)	82.20(8)
S1-Mo1-S3	143.64(3)	140.30(4)	144.42(8)
S1-Mo1-S4	84.95(2)	84.18(5)	84.92(7)
S2-Mo1-S3	85.33(3)	83.62(4)	85.70(8)
S2-Mo1-S4	137.71(3)	141.06(5)	137.78(8)
S3-Mo1-S4	81.99(2)	83.13(6)	81.90(8)

a ref. 19

Table 3

Selected Bond Distances (A) and Angles (deg) of **MoSeL^{Ph} • DMSO**, **MoSeL^{COOMe}** and **MoSeL^{C4H8}**

	MoSeL^{Ph}•DMSO	**MoSeL^{COOMe}**	**MoSeL$^{C4H8, a}$**
Mo1–Se1	2.2915(5)	2.2900(5)	2.3069(5)
Mo1–S1	2.3552(11)	2.3637(11)	2.3517(12)
Mo1–S2	2.3400(10)	2.3645(10)	2.3627(11)
Mo1–S3	2.3520(13)	2.3530(13)	2.3639(11)
Mo1–S4	2.3452(8)	2.3636(13)	2.3618(11)
S1–C1	1.768(3)	1.769(4)	1.786(4)
S2–C2	1.789(5)	1.746(4)	1.770(4)
S3–C3	1.785(3)	1.749(6)	1.772(4)
S4–C4	1.784(4)	1.761(5)	1.765(4)
C1–C2	1.345(5)	1.345(6)	1.331(7)
C3–C4	1.380(7)	1.338(7)	1.338(7)
Mo1–4S plane	0.7976(7)	0.7933(7)	0.79(1)
Se1–Mo1–S1	109.45(3)	109.78(3)	110.86(2)
Se1–Mo1–S2	109.66(3)	109.78(3)	107.59(3)
Se1–Mo1–S3	109.35(3)	108.80(3)	113.20(3)
Se1–Mo1–S4	111.00(3)	110.96(3)	106.50(3)
S1-Mo1-S2	82.09(3)	82.91(3)	82.50(4)
S1-Mo1-S3	141.20(4)	141.41(4)	135.94(4)
S1-Mo1-S4	84.64(3)	84.33(4)	85.77(4)
S2-Mo1-S3	84.56(4)	83.74(4)	84.70(3)
S2-Mo1-S4	139.34(4)	139.99(4)	145.90(3)
S3-Mo1-S4	82.20(3)	83.06(4)	81.78(4)

a ref. 20

Table 4

Selected Bond Distances (A) and Angles (deg) of **MoOL^{Ph}**, **MoOL^{COOMe}** and **MoOL^{C4H8}**

	MoOL^{Ph}	**MoOL$^{COOMe, a}$**	**MoOL$^{C4H8, b}$**
Mo1–O1	1.709(2)	1.686(6)	1.745(6)
Mo1–S1	2.3874(7)	2.380 *c*	2.418(3)
Mo1–S2	2.3761(7)		2.384(7)
Mo1–S3	2.3824(8)		2.418(5)
Mo1–S4	2.3778(7)		2.39(1)
S1–C1	1.792(2)	1.758 *d*	1.76(1)
S2–C2	1.782(3)		1.777(8)
S3–C3	1.785(2)		1.81(1)
S4–C4	1.786(3)		1.783(8)
C1–C2	1.345(4)	1.33(1)	1.34(1)
C3–C4	1.369(5)	1.31(1)	1.32(1)
Mo1–4S–plane	0.7871(5)	e	0.76(1)
O1–Mo1–S1	110.45(8)	108.9 *f*	106.6(4)
O1–Mo1–S2	108.37(7)		106.2(6)
O1–Mo1–S3	110.64(8)		106.5(3)
O1–Mo1–S4	107.04(7)		108.1(4)
S1-Mo1-S2	82.20(2)	83.1(1)	82.4(2)
S1-Mo1-S3	138.89(2)	140.7(1)	146.8(5)
S1-Mo1-S4	86.70(2)	84.3(1)	88.5(4)
S2-Mo1-S3	83.92(2)	85.3(1)	86.7(2)
S2-Mo1-S4	144.57(3)	143.5(1)	145.7(5)
S3-Mo1-S4	82.67(2)	83.0(1)	83.0(4)

a ref. 23,

b ref. 18,

c average distance of the four Mo-S bonds,

d average distance of the four C-S bonds,

e not reported,

f average angle of the four O1-Mo1-S angles.

Table 5

Redox potentials (V vs. SCE) of Mo(V)/Mo(IV) process for **MoEL**

Complexes	L^{COOMe}	L^{Ph}	L^{C4H8}
MoOL	−0.03	−0.46	−0.70
MoSL	−0.12	−0.43	−0.75
MoSeL	−0.12	−0.45	−0.74

Table 6

Solid State Resonance Raman Data (cm^{-1}) for **MoEL^{COOMe}**

Complexes	**ν(Mo≡E)**	**ν(Mo-S)$_{dithiolene}$**	**ν(C=C)$_{sym}$**	**ν(C=O)$_{sym}$**
MoOL^{COOMe}	903	364	1530	1691
MoSL^{COOMe}	493	364	1527	1702
MoSeL^{COOMe}	370[a]	344 [a]	1525	1700

[a] vibrational frequency calculations indicate is significant degree of mixing between ν(Mo≡Se) and ν(Mo-S)$_{ditholene}$ resulting from the small energy difference between these two totally symmetric vibrations.

Table 7

Solution Resonance Raman Data (cm^{-1}) for **MoEL**

Complexes	ν(Mo ≡E) stretch	ν(C=C) stretch
MoOL	897 (L^{C4H8}), 903 (L^{Ph}), 911 (L^{COOMe})[a]	1596 (L^{C4H8}), [c], 1533 (L^{COOMe})
MoSL	480 (L^{C4H8}), 487 (L^{Ph}), 500 (L^{COOMe})	1593 (L^{C4H8}), [c], 1531 (L^{COOMe})
MoSeL	[b] [c] 347 (L^{COOMe})[d]	[b], [c], 1531 (L^{COOMe})

[a] ref. 38.

[b] $MoSeL^{C4H8}$ was decomposed upon irradiation.

[c] not assigned unambiguously.

[d] vibrational frequency calculations indicate both Mo≡Se and $Mo\text{-}S_{dithiolene}$ stretches contribute to the 347 cm^{-1} mode.

Table 8

Percentage Fragment Orbital Character to the Frontier Molecular Orbitals of **MoEL^{COOMe}**

MoOL^{COOMe}				
Molecular Fragment	***% Mo***	***% S$_{dithiolene}$***	***% Dithiolene (total)***	***% Oxo***
HOMO-1	0.8	68.3	95.0	4.1
HOMO	81.2	10.1	18.5	0.3
LUMO	5.9	9.9	90.3	2.8
LUMO+1	3.3	13.5	95.6	0.0
LUMO+2	36.4	7.1	53.9	8.6
LUMO+3	43.3	9.2	45.7	10.2

MoSL^{COOMe}				
Molecular Fragment	***% Mo***	***% S$_{dithiolene}$***	***% Dithiolene (total)***	***% Sulfido***
HOMO-1	0.4	61.0	83.3	15.7
HOMO	80.3	9.8	18.8	0.8
LUMO	21.7	8.7	65.9	11.8
LUMO+1	3.9	13.7	94.4	0.6
LUMO+2	57.7	17.5	22.7	19.5
LUMO+3	39.9	14.4	47.5	12.1

MoSeL^{COOMe}				
Molecular Fragment	***% Mo***	***% S$_{dithiolene}$***	***% Dithiolene (total)***	***% Selenido***
HOMO-1	0.5	56.2	76.6	22.8
HOMO	80.0	9.9	19.1	1.0
LUMO	25.8	8.7	60.0	13.6
LUMO+1	6.2	13.8	91.2	1.7
LUMO+2	55.8	18.2	26.7	17.5
LUMO+3	37.7	15.0	51.4	10.4

Table 9

Band Assignments for Low-Energy Transitions in **MoEL^{COOMe}** Compounds

	MoOL^{COOMe}		**MoSL^{COOMe}**		**MoSeL^{COOMe}**	
Band	***Energy***	***Assignment***	***Energy***	***Assignment***	***Energy***	***Assignment***
1	13,320	HOMO→LUMO	12,750	HOMO→LUMO	12,850	HOMO→LUMO
2	17,720	HOMO→LUMO+1	14,530	HOMO→LUMO+2	14,525	HOMO→LUMO+2
3	21,980	HOMO-1→LUMO	17,242	HOMO-1→LUMO	17,140	HOMO-1→LUMO
4	25,980	HOMO-1→LUMO+1	20,290	HOMO→LUMO+1 HOMO-1→LUMO+2	19,880	HOMO→LUMO+1 HOMO-1→LUMO+2
5		*a*	23,430	HOMO-1→LUMO+1 HOMO-1→LUMO+3	21,180	HOMO-1→LUMO+1 HOMO-1→LUMO+3

a not observed